

Two-leg Su-Schrieffer-Heeger chain with glide reflection symmetry

Shao-Liang Zhang^{1,2} and Qi Zhou^{1,3,*}

¹*Department of Physics, The Chinese University of Hong Kong, Shatin, New Territories, Hong Kong*

²*School of Physics, Huazhong University of Science and Technology, Wuhan 430074, China*

³*Department of Physics and Astronomy, Purdue University, West Lafayette, Indiana 47907, USA*

(Received 24 May 2016; published 23 June 2017)

The Su-Schrieffer-Heeger (SSH) model lays the foundation of many important concepts in quantum topological matters. Here, we show that a spin-dependent double-well optical lattice allows one to couple two topologically distinct SSH chains in the bulk and realize a glided-two-leg SSH model that respects the glide reflection symmetry. Such a model gives rise to intriguing quantum phenomena beyond the paradigm of a traditional SSH model. It is characterized by Wilson lines that require non-Abelian Berry connections, and the interplay between the glide symmetry and interaction automatically leads to charge fractionalization without jointing two lattice potentials at an interface. Our work demonstrates the versatility of ultracold atoms to create new theoretical models for studying topological matters.

DOI: 10.1103/PhysRevA.95.061601

The beauty of the Su-Schrieffer-Heeger(SSH) model [1,2] is reflected by its extremely simple form that well captures a variety of deep concepts lying at the heart of modern condensed matter physics. Such a model describes a one-dimensional chain, which is characterized by two tunneling amplitudes t_1 and t_2 between two sublattices A and B . The SSH model serves as a textbook example for discussing the Zak phase, an Abelian geometric phase that characterizes distinct topological phases in one dimension, and zero-energy end states in a finite system with open boundaries [3–6]. It is also a prototypical model for studying fractionalized charges, one of the most exotic phenomena in quantum systems, if interfaces exist in the lattice potential to separate topologically distinct chains into multiple domains in the real space [7,8].

Ultracold atoms have emerged as a highly controllable platform for simulating topological models that are difficult to access in solids [9–14]. The double-well optical lattice [15–17], which is composed of a long and a short lattice, has been demonstrated as a powerful tool to explore the SSH model. It has been used to measure the Zak phases [18] and to realize topological charge pumping [19,20]. Despite the aforementioned exciting progress, a question naturally arises on whether physicists could use ultracold atoms to explore new theoretical models other than simulating those readily available in the literature, such as topological matters characterized by non-Abelian Berry curvatures and connections. Nonsymmorphic symmetries have recently attracted a lot of interest in the condensed matter communities. Such symmetries give rise to band crossing points in the energy spectra. The band crossing points invalidate the application of Abelian Berry curvature and connections, and the topological properties of the system should be described by non-Abelian Berry curvatures and connections [21,22]. However, systematic studies of nonsymmorphic symmetries in ultracold atoms are lacking [23].

In this Rapid Communication, we show that a spin-dependent optical double-well lattice allows one to realize

a glided-two-leg SSH model, which is composed of two one-dimensional SSH chains shifted from each other by half of the lattice spacing, as shown in Figs. 1(a) and 1(b). Unlike the conventional means of linking two topologically distinct chains at an interface, the two chains here are coupled in the bulk, and provide a unique playground to explore the interplay between topology, symmetry, and interaction. The theoretical description of the system is fundamentally different from that for traditional SSH. Because of band touching points, which are protected by the glide symmetry [24–26], in the Brillouin zone (BZ), the conventional Abelian geometric phase is no longer capable of describing the topological properties. Non-Abelian Berry connections and Wilson lines are inevitably required [27]. Such a Wilson line can be measured using strong-force dynamics in Bloch bands, as shown by the recent experiment done by Bloch's group [28]. By introducing interactions to the system, even more interesting phenomena arise. A repulsive interaction gives rise to a ferromagnet at half filling. Without resorting to producing domains in the lattice potential, doping the ferromagnet naturally leads to the splitting of an extra particle into two deconfined domain walls, each of which carries half of the charge of the extra particle [29–33]. Such a fractionalized charge can be easily manipulated as mobile or localized ones, and are directly observable using standard in-site density images of atoms.

Spin-dependent double-well lattice. We consider the Hamiltonian of two hyperfine spin states of fermions in a spin-dependent double-well lattice in the presence of a microwave coupling,

$$\hat{H} = \int dx [\hat{\psi}_\sigma^\dagger(x) \hat{H}_\sigma \hat{\psi}_\sigma(x) + \Omega (\hat{\psi}_\uparrow^\dagger(x) \hat{\psi}_\downarrow(x) + \text{H.c.})], \quad (1)$$

where

$$\hat{H}_\sigma(x) = \frac{\hat{p}^2}{2m} - V_S \cos^2\left(\frac{2\pi x}{d}\right) + 2V_L \sigma_z \sin\left(\frac{2\pi x}{d}\right), \quad (2)$$

$\sigma = \uparrow, \downarrow$ characterize the hyperfine spin, $\sigma_z = \pm \frac{1}{2}$, d is the lattice spacing, and $V_S > 0$ and V_L are the lattice depths of the short and long lattices, respectively. The long lattice

*Corresponding author: zhou753@purdue.edu

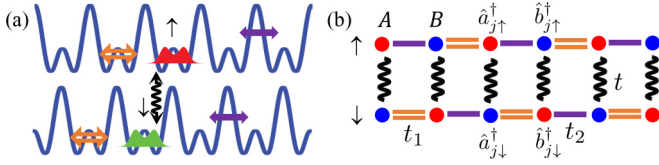


FIG. 1. Glided-two-leg SSH model in a spin-dependent optical lattice. (a) Spin-up (red color) and spin-down atoms (green color) are loaded in two different double-well lattices, each of which is shifted from the other by half of the lattice spacing $d/2$. A microwave field provides an interleg tunneling t (wiggles). The single (purple) and double (orange) lines represent two tunnelings t_1 and t_2 , respectively. (b) Tight-binding model. Red (dark gray) and blue (black) dots represent different sublattice sites, respectively.

potential is red and blue detuned for the spin-up and spin-down atoms, respectively, and thus depends on σ_z [34]. As shown in Fig. 1(a), $\hat{H}_\sigma(x)$ describes a standard double-well lattice, each of which shifts in a spin-dependent way from the other by half of the lattice spacing $d/2$. Ω is the strength of a microwave field, which couples these two hyperfine spin states [35]. Such a system resembles polyacetylene with an opposite dimerization between nearest-neighbor chains [36]. There are many alternative ways of coupling two hyperfine spin states instead of a microwave field, for example, rf spectroscopy to couple different internal states of the atoms or by using a narrow optical transition in alkaline-earth-like atoms. There is an alternative scheme to realize an equivalent model (see the Supplemental Material [37]).

A tight-binding model can be constructed straightforwardly, as shown in Fig. 1(b),

$$\hat{H}_L = \sum_j [t_1(\hat{a}_{j\uparrow}^\dagger \hat{b}_{j\uparrow} + \hat{b}_{j\downarrow}^\dagger \hat{a}_{j+1\downarrow}) + t_2(\hat{b}_{j\uparrow}^\dagger \hat{a}_{j+1\uparrow} + \hat{a}_{j\downarrow}^\dagger \hat{b}_{j\downarrow})] + t \sum_j (\hat{a}_{j\uparrow}^\dagger \hat{a}_{j\downarrow} + \hat{b}_{j\uparrow}^\dagger \hat{b}_{j\downarrow}) + \text{H.c.}, \quad (3)$$

where $\hat{a}_{j\sigma}^\dagger$ and $\hat{b}_{j\sigma}^\dagger$ are the creation operators for spin-up or spin-down atoms at the left and right wells on site j , t_1 and t_2 are the intraleg tunneling, and t is the interleg tunneling. In this Rapid Communication, j is reserved for the site index of the double-well lattice, each of which corresponds to two wells. Apparently, each leg is a conventional SSH model. t_1 and t_2 switch positions in these two legs due to the relative shift of half of the lattice spacing. These two legs with opposite dimerizations correspond to two topologically distinct configurations of a single SSH model regardless of the location of the boundary.

The bulk spectrum can be obtained straightforwardly. We find out that the two lowest (highest) bands touch at the zone boundary, regardless of the value of t . Figure 2(a) shows a typical band structure. The band touching points originate from the glide reflection symmetry of the Hamiltonian. Under a transformation that is a combination of the spin flip $\uparrow \leftrightarrow \downarrow$ and a spatial translation of half of the lattice spacing $d/2$, the Hamiltonian in (1) is invariant. If the spin is viewed as a synthetic dimension along the y direction, this invariance exactly corresponds to a glide reflection symmetry. Such symmetry is crucial for certain types of topological superfluids

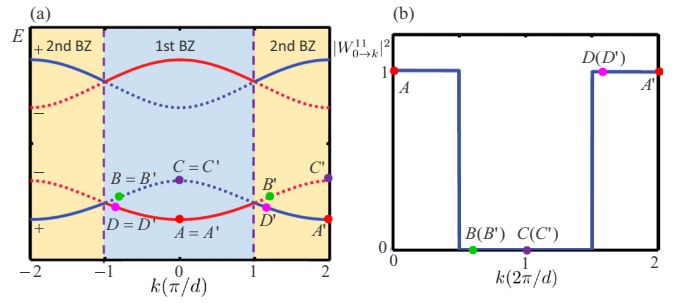


FIG. 2. Band structure, Bloch oscillation, and Wilson line. (a) Band structure and Bloch oscillation. The light blue and yellow regions correspond to the first and second BZ, respectively. The first, second, third, and fourth bands are represented by solid, dotted, dotted, and solid curves, respectively. The $-$ (red) and $+$ (blue) branches of the eigenstates of the glide operator are distinguished by colors. In the presence of an external force, a particle starting from A in the first band crosses the zone boundary and enters the second band in the second BZ (point B' , which is identical to B). After traveling for one reciprocal lattice vector $2\pi/d$, the particle ends at C , a state orthogonal to the initial one at A . After another reciprocal lattice vector $2\pi/d$, the particle returns to A . The primes in symbols $A'-D'$ represent the different signs of η in the second BZ from the first BZ. (b) Wilson line. When a particle initially stays at the first band, $|W_{0\rightarrow k}^{11}|^2$ corresponds to the probability of the particle to remain at this band. Since the electric field cannot couple the $+$ and $-$ branches, $|W_{0\rightarrow k}^{11}|^2$ remains as 1 or 0 unless crossing the zone boundary.

and crystalline insulators [24–26]. Here, glide reflection symmetry naturally emerges from the spin-dependent lattice.

The glide operator is explicitly written as

$$\hat{G}_k = e^{\frac{ikd}{2}} \left(\cos \frac{kd}{2} \sigma_x \tau_x + \sin \frac{kd}{2} \sigma_x \tau_y \right), \quad (4)$$

where σ and τ are Pauli matrices, and the pseudospin $\tau_z = \pm 1$ describe states on sublattices A and B , respectively. As \hat{G}_k^2 is a translation for one lattice spacing, and $\hat{G}_k^2 |\psi_{k,n}\rangle = e^{ikd} |\psi_{k,n}\rangle$, one sees that the eigenvalues of \hat{G}_k are $\pm e^{ikd/2}$. The periodicity of these eigenvalues are $4\pi/d$, twice that of the Hamiltonian. We use $\eta = \pm$ to distinguish these two different eigenvalues and the corresponding eigenstates. In the system with glide symmetry, all bands must appear in pairs with opposite signs of η , as shown in Fig. 2(a). When $k \rightarrow k + 2\pi/d$, η changes sign. Thus a band crossing point must exist. We should point out that glide symmetry does not ensure that the band crossing point appears at the edge of BZ. In this system, there is also a mirror symmetry, and the Hamiltonian (1) is conserved with the translation $x \rightarrow -x$, $\uparrow \leftrightarrow \downarrow$. The mirror operator \hat{M} satisfies the relation $\hat{M} \hat{G}_k \hat{T}_d = \hat{G}_k \hat{M}$, where \hat{T}_d is the translation for one lattice spacing d . Thus, \hat{M} anticommutes with the glide operator \hat{G} at $k = \pm\pi/d$, and gives rise to the band touching points at the zone boundary. Similar to Ref. [24], in the presence of an additional symmetry, the mirror reflection with respect to the center of the A - B bond here, such a band touching point must appear at the zone boundary $\pm\pi/d$. As shown in Fig. 2, the first, second, third, and fourth bands in the first BZ have $\eta = -, +, +, -$, respectively. Due to the band touching point at the zone boundary, these four bands

have $\eta = +, -, -, +$ in the second BZ, respectively. The band touching point can also be understood by an alternative way (see the Supplemental Material [37]). When the mirror symmetry is broken, the band crossing points could show up in other places in the BZ. In particular, when t becomes complex, tuning the phase of t allows one to move the band crossing points in BZ.

Wilson line. The glide-symmetry-protected band touching points tell one that the Abelian geometric phase is no longer applicable to describe the topological states in the system, unlike the traditional single SSH chain. A Wilson line must be required to characterize the topological properties [27]. Using the periodic Bloch wave function $|u_{k,1}\rangle = e^{-ikx}|\psi_{k,1}\rangle$ and $|u_{k,2}\rangle = e^{-ikx}|\psi_{k,2}\rangle$, the Wilson line that describes the two lowest bands is written as

$$\hat{W}_{k \rightarrow k + \frac{2\pi}{d}} = \hat{P} \exp \left(i \int_k^{k + \frac{2\pi}{d}} dq \hat{A}(q) \right), \quad (5)$$

where \hat{P} is the path ordering operator and the matrix representation $\hat{A}(q) = i \langle u_{q,m} | \partial_q | u_{q,n} \rangle$, where $m, n = 1, 2$ is the band index. It has been shown both theoretically [38] and experimentally [28] that such a Wilson line can be measured using Bloch oscillations of ultracold atoms in the limit $w \ll Fd \ll E_G$, where F is the effective electric field force, w is the total bandwidth of the lowest two bands, and E_G is the energy separation between the two lowest and highest bands. In such a limit, the transition to the two highest bands, as well as the dispersions of the two lowest bands, is negligible, so that the dynamics is well characterized by $\hat{W}_{k \rightarrow k + \frac{2\pi}{d}}$. Under the effective electric field Fx , the time evolution of the momentum follows $\hbar dq/dt = F$, and $|W_{k \rightarrow k + \frac{2\pi}{d}}^{mn}|^2 \equiv |\langle u_{k,m} | \hat{W}_{k \rightarrow k + \frac{2\pi}{d}} | u_{k,n} \rangle|^2$ describes the probability of having the particle in the m th band after an evolution circle $k \rightarrow k + 2\pi/d$ if the particle is initially prepared in the n th band.

Through an explicit calculation, we find that η is conserved in the Bloch oscillation (see the Supplemental Material [37]). Meanwhile, since $\eta = \pm$ is associated with the first and the second bands, which are represented by the solid and dotted curves in Fig. 2(a), respectively, they switch with each other across the zone boundary. In the adiabatic limit, where $Fd \ll E_G$, the wave function accumulates a phase in such an oscillation, i.e., $|u_{k,\pm}\rangle \rightarrow e^{i\varphi_{\pm}} |u_{k',\pm}\rangle$, when $k \rightarrow k'$, whereas φ_{\pm} is gauge dependent if $k - k' \neq 0 \pmod{4\pi/d}$, and it gives rise to the well-known Zak phase φ_{Zak} when $k \rightarrow k + 4\pi/d$, which is π or 0 depending on whether t is smaller or larger than $|t_1 + t_2|$, as that in a standard hybridized s - p model with a lattice spacing $d/2$ [39–41].

We now return to the question about the form of $\hat{W}_{k \rightarrow k + 2\pi/d}$, whose matrix form needs to be evaluated in the basis $|u_{1,k}\rangle$ and $|u_{2,k}\rangle$ so that $|\psi_{1,k}\rangle$ and $|\psi_{2,k}\rangle$ have a periodicity $2\pi/d$. From the discussion above, one obtains the Wilson line for $k \rightarrow k + 2\pi/d$,

$$(W_{k \rightarrow k + \frac{2\pi}{d}}^{mn}) = \begin{pmatrix} 0 & e^{i\varphi_+} \\ e^{i\varphi_-} & 0 \end{pmatrix}, \quad (6)$$

though neither φ_+ nor φ_- is well defined individually, since $k \rightarrow k + 2\pi/d$ finishes only half of one period of \pm bands,

which is $4\pi/d$, as aforementioned. We can define $\varphi_+ + \varphi_- = \varphi_{\text{Zak}}$ as the total geometric phase accumulated in the evolution, which can be easily understood from the fact that both $|u_{1,k}\rangle \rightarrow e^{i\varphi_+} |u_{2,k}\rangle$ and $|u_{2,k}\rangle \rightarrow e^{i\varphi_-} |u_{1,k}\rangle$ are satisfied when k increases by $2\pi/d$ across the band touching point. Thus we obtain

$$(W_{k \rightarrow k + \frac{2\pi}{d}}^{mn}) = e^{i\varphi_{\text{Zak}}/2} \begin{pmatrix} 0 & e^{i\varphi_r} \\ e^{-i\varphi_r} & 0 \end{pmatrix}, \quad (7)$$

where $\varphi_r = (\varphi_+ - \varphi_-)/2$. Equation (7) clearly shows the non-Abelian nature of the geometric phase here, since $|u_{1,k}\rangle$ and $|u_{2,k}\rangle$ have to exchange with each other when $k \rightarrow k + 2\pi/d$, resembling a Möbius strip [24,26,42]. It also tells one that $\hat{W}_{k \rightarrow k + \frac{2\pi}{d}}$ can be decomposed to a U(1) phase $e^{i\varphi_{\text{Zak}}/2}$ and a SU(2) transformation corresponding to rotating a pseudospin- $\frac{1}{2}$ formed by the two lowest bands. Thus, it topologically corresponds to a Möbius strip, which may also emerge in other systems with glide symmetry [24,26,42,43]. Alternatively, if considering $k \rightarrow k + 4\pi/d$, i.e., the momentum finishes two circles, one concludes

$$(W_{k \rightarrow k + \frac{4\pi}{d}}^{mn}) = \begin{pmatrix} e^{i\varphi_{\text{Zak}}} & 0 \\ 0 & e^{i\varphi_{\text{Zak}}} \end{pmatrix} = e^{i\varphi_{\text{Zak}}} \mathcal{I}, \quad (8)$$

i.e., the Wilson line becomes an identity matrix \mathcal{I} .

Both Eqs. (7) and (8) are verified by numerical simulations of the dynamics in the four-band model (see the Supplemental Material [37]). The populations in different bands are shown in Fig. 2(b), if a particle is initially prepared at state $|u_{k,1}\rangle$ or $|u_{k,2}\rangle$. The populations approach the step functions and acquire sudden jumps at $k = \pi/d$ and $k = 3\pi/d$, which directly confirm the prediction of Eqs. (7) and (8). The phases φ_+ and φ_- can also be measured directly in experiments using the same interferometric method that has been applied by Bloch's group [28]. As mentioned above, interleg tunneling provides one additional degree of freedom to control the topological properties, since the total phase $\varphi_+ + \varphi_-$ has a π difference across the topological transition point $t_c = |t_1 + t_2|$. On both sides of the transition point, the SU(2) part of the Wilson line exists, and the difference comes from the U(1) part, i.e., a $\pi/2$ difference in the total phase. In a conventional topologically nontrivial SSH chain, the Zak phase is π . Here, the $\pi/2$ phase is a consequence of the non-Abelian nature of the topological bands of our two-leg SSH chains. This difference will induce the disappearance of the edge state when the open boundary condition is applied (detailed discussions of the edge states are presented in the Supplemental Material [37]). It is also worth mentioning that the absolute value of the eigenvalue of a unitary matrix is one. Thus the phases of the eigenvalues of the Wilson line ($W_{k \rightarrow k + \frac{2\pi}{d}}^{mn}$) allow one to distinguish different topological phases. When $t < t_c$, the two eigenvalues are $\pm i$, and the phases of the two eigenvalues are always $\pm\pi/2$, respectively. When $t > t_c$, the two eigenvalues become ± 1 , i.e., the phases become π and 0 , respectively.

Charge fractionalization. We consider an on-site repulsive interaction,

$$\hat{V} = U \sum_j (\hat{n}_{j,a\uparrow} \hat{n}_{j,a\downarrow} + \hat{n}_{j,b\uparrow} \hat{n}_{j,b\downarrow}), \quad (9)$$

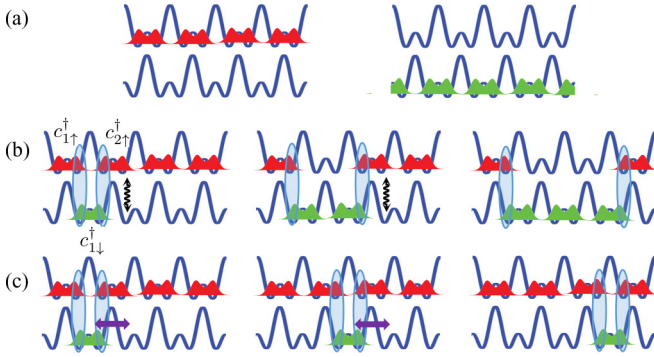


FIG. 3. Charge fractionalization. (a) At half filling, a repulsive interaction leads to spontaneous symmetry breaking and a ferromagnet emerges. The red (dark gray) and green (light gray) clouds represent the Wannier wave functions of the spin-up and spin-down particles, respectively. (b) Doping an extra particle forms two domain walls (blue ovals). If $t_2 = 0$, the two domain walls are deconfined because of interchain tunneling t (black wiggles). (c) If $t = 0$, the two domain walls are confined for any finite intrachain tunneling t_2 (purple arrow).

where $U > 0$ is the on-site interaction strength. In the extreme case $t_2 = t = 0$, flatbands arise. Localized orbitals $\hat{c}_{j\uparrow}^\dagger|0\rangle = (\hat{a}_{j\uparrow}^\dagger + \hat{b}_{j\uparrow}^\dagger)|0\rangle/\sqrt{2}$ and $\hat{c}_{j\downarrow}^\dagger|0\rangle = (\hat{b}_{j\downarrow}^\dagger + \hat{a}_{j+1\downarrow}^\dagger)|0\rangle/\sqrt{2}$ are the degenerate eigenstates of this flatband with energy t_1 . Since $t_1 < 0$ is chosen, the high-energy states $(\hat{a}_{j\sigma}^\dagger - \hat{b}_{j\sigma}^\dagger)|0\rangle/\sqrt{2}$ are not relevant in the low-energy limit, provided that $|t|$, $|t_2|$, and U are much smaller than $|t_1|$. In such a flatband limit, a ferromagnet naturally emerges at half filling, i.e., all atoms fill up either the spin-up or spin-down chain, as shown in Fig. 3(a), since it saves the interaction energy and meanwhile does not cost extra kinetic energy in a flatband. In other words, a repulsive interaction lifts the single-particle degeneracy. Clearly, such a ferromagnet has a twofold degeneracy, and the ground state can be $|G\rangle_1 = \prod_j \hat{c}_{j\uparrow}^\dagger|0\rangle$ or $|G\rangle_2 = \prod_j \hat{c}_{j\downarrow}^\dagger|0\rangle$.

In the presence of small t_2 and t , it is expected that the ferromagnet is protected by the gap given by the repulsive interaction. We use the time-evolving block decimation (TEBD) algorithm [44,45] to numerically obtain the ground state at half filling. For a wide range of realistic lattice parameters, we have found that a ferromagnet emerges in the parameter regime $|t_2|, |t| \ll U \ll |t_1|$. For instance, the critical value of the interaction strength in Fig. 3 is $U_c = 0.03E_R$. In terms of temperature, the gap is about 5 nK, which is accessible in current experiments.

Now consider that by adding one more atom to one of the spontaneous symmetry-breaking ground states $|G\rangle_1$, in the limit that $U \ll |t_1|$, an extra particle prefers to occupy the spin-down chain to avoid the large kinetic energy penalty, which is of the order of $|t_1|$, caused by occupying an atomic orbital $(\hat{a}_{j\uparrow}^\dagger - \hat{b}_{j\uparrow}^\dagger)|0\rangle/\sqrt{2}$. As shown in Figs. 3(b) and 3(c), such an extra particle creates two domain walls. A natural question is then, are these two domain walls confined with each other or they are deconfined? Two extreme cases are rather simple. When $t_2 = 0$ and $t \neq 0$, both spin-up atoms that have a spatial overlap with the extra spin-down atoms can tunnel to the spin-down chain to gain the kinetic energy from the interleg tunneling. Interestingly, such a tunneling does not cost any

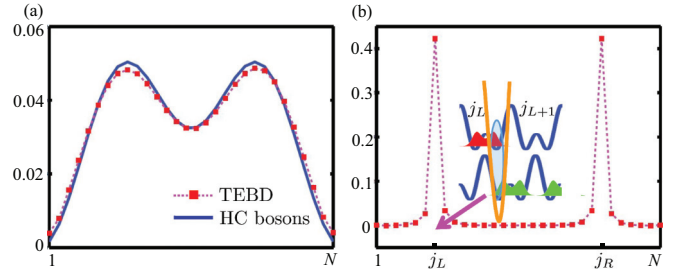


FIG. 4. The distribution of the extra particle. The parameters used in the TEBD simulation are $t_1 = -0.4E_R$, $t_2 = -4 \times 10^{-4}E_R$, $t = 8 \times 10^{-4}E_R$, and $U = 0.012E_R$. The lattice site is $N = 30$ with an open boundary condition. (a) For deconfined domain walls, the result of the TEBD simulation agrees with the density distribution of two hard-core particles (blue). (b) The additional local potential $V_L = V_R = -0.002E_R$ (yellow curve). When two deconfined domain walls are localized at the right well of the lattice site $j_L = 7$ and the left well of the lattice site $j_R = 24$, the extra particle density is centered around these two lattice sites.

interaction energy, since the number of domain walls remains as 2. Such progress continuously occurs, and these two domain walls become deconfined so that the length of the spin-down domain becomes arbitrary, as shown in Fig. 3(b). One thus concludes that each domain wall carries $\frac{1}{2}$ of the charge of the extra particle. Such fractionalization is naturally induced by the interplay between the interaction and the glide symmetry of the noninteracting Hamiltonian, so that it is not required to create an interface in the lattice potential to separate topologically distinct phases. In contrast, if $t = 0$ and $t_2 \neq 0$, what is relevant is the tunneling of a single spin-down atom in the spin-down chain. Clearly, two domain walls are always confined with each other, as shown in Fig. 3(c). In such a confined state, charge is not fractionalized. For generic cases with finite t and t_2 , we find both analytically and numerically a first-order phase transition between the confined and deconfined states at a critical value $t_2 = 2t$, due to the competition between the two energy scales (see the Supplemental Material [37]).

The deconfined domain walls can be traced from the density distribution of an additional particle $\tilde{n}_j = n_j - 1$. The result of the TEBD method is shown in Fig. 4(a). In the deconfined phase, two domain walls move freely and the only constraint is that they cannot penetrate each other. As a result, \tilde{n}_j resembles the density distribution of two free hard-core particles in one dimension. In contrast, in the confined phase, two domain walls are tightly bound with each other, and \tilde{n}_j resembles the density distribution of a molecule, whose size is d .

One can also introduce a local potential to pin down the domain walls in certain lattice sites. Applying a localized laser beam, the lattice potential becomes deeper at two lattice wells, say, the right well of j_L and the left well of j_R . Whereas the localized potential may also change the on-site interaction strength at sites j_L and j_R , the leading contribution is the potential energy gained ϵ . Each domain wall, which corresponds to some extra particle numbers, prefers to occupy these two sites to gain the energy ϵ , the potential energy produced by the deep local potentials V_L and V_R . Define $\Delta n_j = n_j - n_j^0$, where $n_j^0 = 1$ is the particle number per lattice site (including two wells) of the ferromagnet at half

filling. The result of TEBD shows that Δn_j is indeed peaked around j_L and j_R , as shown in Fig. 4(b). The width of the peak ξ depends on the ratio J/ϵ . Choosing the distance between two localized potentials $|j_L - j_R| \gg \xi$, one could compute the total extra charge in the left and right side of the system,

$$\Delta N_L = \sum_{i=1}^{N/2} \Delta n_j, \quad \Delta N_R = \sum_{i=N/2+1}^N \Delta n_j, \quad (10)$$

and we indeed find out that $\Delta N_L = \Delta N_R = \frac{1}{2}$. In the strong localization limit, $J \ll \epsilon$ and $\xi \sim d$, $\Delta N_L \approx \Delta n_{j_L}$ and $\Delta N_R \approx \Delta n_{j_R}$, and the fractionalized charge- $\frac{1}{2}$ localized at sites j_L and j_R . To further confirm such a fractionalized charge- $\frac{1}{2}$, we compute the number fluctuation in the left and right half of the system, and have found out that the number fluctuation is zero. In the strong localization limit, this is equivalent to the number fluctuation at the site j_L or j_R . Such an observation distinguishes the fractionalized charge- $\frac{1}{2}$ from the trivial one produced by a single particle hopping between two lattice sites, where the average occupation in each site is

also $\frac{1}{2}$ and the charge fluctuation is of the same order. Whereas we have been focusing on well-localized potentials V_L and V_R , which is achievable in current experiments, in practice, a potential with a width of a few lattice spacing also works, since it only quantitatively affects the width of the density peaks.

Whereas we have been focusing on ideal double-well lattices, all results can be straightforwardly generalized to cases with perturbations (see the Supplemental Material [37]). Since the study of new topological matters is currently one of the main themes in both condensed matter and ultracold atom physics [46–51], we hope that our work may stimulate more studies on the interplay between glide symmetry, topology, and interactions using highly controllable ultracold atomic samples.

We acknowledge useful discussions with I. Bloch, E. Mueller, and C. X. Liu. We credit J. Zhang for asking the question on the Hamiltonian of a Raman dressed lattice that inspired us to consider the equivalent Hamiltonian \hat{H}' . This work is supported by National Natural Science Foundation of China (NSFC)/Research Grants Council (RGC) Joint Research Scheme (NCUHK453/13).

-
- [1] W. P. Su, J. R. Schrieffer, and A. J. Heeger, *Phys. Rev. Lett.* **42**, 1698 (1979).
- [2] S. Q. Shen, *Topological Insulators: Dirac Equation in Condensed Matters* (Springer, Berlin, 2012).
- [3] J. Zak, *Phys. Rev. Lett.* **62**, 2747 (1989).
- [4] R. Jackiw and C. Rebbi, *Phys. Rev. D* **13**, 3398 (1976).
- [5] S. A. Brazovskii, *Pis'ma Zh. Eksp. Teor. Fiz.* **28**, 856 (1978) [*Sov. Phys. JETP Lett.* **28**, 606 (1978)].
- [6] M. J. Rice, *Phys. Lett. A* **71**, 152 (1979).
- [7] M. J. Rice and E. J. Mele, *Phys. Rev. Lett.* **49**, 1455 (1982).
- [8] A. J. Heeger, S. Kivelson, J. R. Schrieffer, and W. P. Su, *Rev. Mod. Phys.* **60**, 781 (1988).
- [9] M. Aidelsburger, M. Atala, M. Lohse, J. T. Barreiro, B. Paredes, and I. Bloch, *Phys. Rev. Lett.* **111**, 185301 (2013).
- [10] H. Miyake, G. A. Siviloglou, C. J. Kennedy, W. C. Burton, and W. Ketterle, *Phys. Rev. Lett.* **111**, 185302 (2013).
- [11] G. Jotzu, M. Messer, R. Desbuquois, M. Lebrat, T. Uehlinger, D. Greif, and T. Esslinger, *Nature (London)* **515**, 237 (2014).
- [12] L. Huang, Z. Meng, P. Wang, P. Peng, S. L. Zhang, L. Chen, D. Li, Q. Zhou, and J. Zhang, *Nat. Phys.* **12**, 540 (2016).
- [13] N. Fläschner, B. S. Rem, M. Tarnowski, D. Vogel, D. S. Lühmann, K. Sengstock, and C. Weitenberg, *Science* **352**, 1091 (2016).
- [14] Z. Wu, L. Zhang, W. Sun, X. T. Xu, B. Z. Wang, S. C. Ji, Y. Deng, S. Chen, X. J. Liu, and J. W. Pan, *Science* **354**, 83 (2016).
- [15] J. Sebby-Strabley, M. Anderlini, P. S. Jessen, and J. V. Porto, *Phys. Rev. A* **73**, 033605 (2006).
- [16] N. Lundblad, P. J. Lee, I. B. Spielman, B. L. Brown, W. D. Phillips, and J. V. Porto, *Phys. Rev. Lett.* **100**, 150401 (2008).
- [17] S. Trotzky, P. Cheinet, S. Fölling, M. Feld, U. Schnorrberger, A. M. Rey, A. Polkovnikov, E. A. Demler, M. D. Lukin, and I. Bloch, *Science* **319**, 295 (2008).
- [18] M. Atala, M. Aidelsburger, J. T. Barreiro, D. Abanin, T. Kitagawa, E. Demler, and I. Bloch, *Nat. Phys.* **9**, 795 (2013).
- [19] M. Lohse, C. Schweizer, O. Zilberberg, M. Aidelsburger, and I. Bloch, *Nat. Phys.* **12**, 350 (2016).
- [20] S. Nakajima, T. Tomita, S. Taie, T. Ichinose, H. Ozawa, L. Wang, M. Troyer, and Y. Takahashi, *Nat. Phys.* **12**, 296 (2016).
- [21] S. M. Young and C. L. Kane, *Phys. Rev. Lett.* **115**, 126803 (2015).
- [22] Y. X. Zhao and A. P. Schnyder, *Phys. Rev. B* **94**, 195109 (2016).
- [23] H. Chen, X. J. Liu, and X. C. Xie, *Phys. Rev. A* **93**, 053610 (2016).
- [24] Q. Z. Wang and C. X. Liu, *Phys. Rev. B* **93**, 020505(R) (2016).
- [25] C. Fang and L. Fu, *Phys. Rev. B* **91**, 161105(R) (2015).
- [26] K. Shiozaki, M. Sato, and K. Gomi, *Phys. Rev. B* **91**, 155120 (2015).
- [27] F. Wilczek and A. Zee, *Phys. Rev. Lett.* **52**, 2111 (1984).
- [28] T. Li, L. Duca, M. Reitter, F. Grusdt, E. Demler, M. Endres, M. Schleier-Smith, I. Bloch, and U. Schneider, *Science* **352**, 1094 (2016).
- [29] R. B. Laughlin, *Phys. Rev. Lett.* **50**, 1395 (1983).
- [30] J. Martin, S. Ilani, B. Verdene, J. Smet, V. Umansky, D. Mahalu, D. Schuh, G. Abstreiter, and A. Yacoby, *Science* **305**, 980 (2004).
- [31] K. Behnia, L. Balicas, and Y. Kopelevich, *Science* **317**, 1729 (2007).
- [32] H. Steinberg, G. Barak, A. Yacoby, L. N. Pfeiffer, K. W. West, B. I. Halperin, and K. L. Hur, *Nat. Phys.* **4**, 116 (2008).
- [33] M. Leder, C. Grossert, L. Sitta, M. Genske, A. Rosch, and M. Weitz, *Nat. Commun.* **7**, 13122 (2016).
- [34] O. Mandel, M. Greiner, A. Widera, T. Rom, T. W. Hänsch, and I. Bloch, *Phys. Rev. Lett.* **91**, 010407 (2003).
- [35] A. G. Martin, K. Helmerson, V. S. Bagnato, G. P. Lafyatis, and D. E. Pritchard, *Phys. Rev. Lett.* **61**, 2431 (1988).
- [36] D. Baeriswyl and K. Maki, *Phys. Rev. B* **28**, 2068 (1983).

- [37] See Supplemental Material at <http://link.aps.org/supplemental/10.1103/PhysRevA.95.061601> for a few schemes to realize \hat{H}' , an alternative way to understand the band touching point, the absence of a transition between the + and - branches of the eigenstates of the glide operator, the topological phase transition at the critical point $t_c = |t_1 + t_2|$, the effective Hamiltonian for domain walls and first-order phase transitions, and the effect of the perturbations.
- [38] F. Grusdt, D. Abanin, and E. Demler, *Phys. Rev. A* **89**, 043621 (2014).
- [39] X. Li, E. Zhao, and W. V. Liu, *Nat. Commun.* **4**, 1523 (2013).
- [40] W. Zheng and H. Zhai, *Phys. Rev. A* **89**, 061603(R) (2014).
- [41] S. L. Zhang and Q. Zhou, *Phys. Rev. A* **90**, 051601(R) (2014).
- [42] S. N. Ji, B. F. Zhu, and R. B. Liu, [arXiv:1305.5289](https://arxiv.org/abs/1305.5289).
- [43] B. Wang, Z. Zheng, H. Pu, X. Zou, and G. Guo, *Phys. Rev. A* **93**, 031602(R) (2016).
- [44] G. Vidal, *Phys. Rev. Lett.* **93**, 040502 (2004).
- [45] M. L. Wall and L. D. Carr, Open Source TEBD, <https://inside.mines.edu/lcarr/software.html> (2009).
- [46] L. Fu, *Phys. Rev. Lett.* **106**, 106802 (2011).
- [47] P. Dziawa, B. J. Kowalski, K. Dybko, R. Buczko, A. Szczerbakow, M. Szot, E. Łusakowska, T. Balasubramanian, B. M. Wojek, M. H. Berntsen, O. Tjernberg, and T. Story, *Nat. Mater.* **11**, 1023 (2012).
- [48] Y. Tanaka, Z. Ren, T. Sato, K. Nakayama, S. Souma, T. Takahashi, K. Segawa, and Y. Ando, *Nat. Phys.* **8**, 800 (2012).
- [49] Y. Okada, M. Serbyn, H. Lin, D. Walkup, W. Zhou, C. Dhital, M. Neupane, S. Xu, Y. J. Wang, R. Sankar, F. Chou, A. Bansil, M. Z. Hasan, S. D. Wilson, L. Fu, and V. Madhavan, *Science* **341**, 1496 (2013).
- [50] Y. Kim, C. L. Kane, E. J. Mele, and A. M. Rappe, *Phys. Rev. Lett.* **115**, 086802 (2015).
- [51] Y. Ando and L. Fu, *Annu. Rev. Condens. Matter Phys.* **6**, 361 (2015).